energies

MDPI

Article

Sensorless Control of Voltage Peaks in Class-E Single-Ended Resonant Inverter for Induction Heating Rice Cooker

Yongseung Oh [1], Jaeeul Yeon [2], Jayoon Kang [3], Ilya Galkin [4], Wonsoek Oh [5] and Kyumin Cho [6,*]

1 R&D Center, Willings Co., Ltd., Yongin-si 17037, Gyeonggi-do, Korea; ysoh@willings.co.kr
2 Infineon Technologies Austria AG, 9500 Villach, Austria; dionisus@naver.com
3 Department of Mechatronics Engineering, Hanyang University, Seongdong-gu, Seoul 04763, Korea; jykang@keti.re.kr
4 Institute of Industrial Electronics and Electrical Engineering, Riga Technical University, LV-1658 Riga, Latvia; gia@eef.rtu.lv
5 Department of Electrical Engineering, Yuhan University, Bucheon 14780, Gyeonggi-do, Korea; oppa@yuhan.ac.kr
6 Department of Information and Communication Engineering, Yuhan University, Bucheon 14780, Gyeonggi-do, Korea
* Correspondence: limsa@yuhan.ac.kr; Tel.: +82-10-3727-5498

Abstract: Single-ended (SE) resonant inverters are widely used as power converters for high-pressure rice cooker induction, with 1200 V insulated-gate bipolar transistors (IGBTs) being used as switching devices for kW-class products. When voltage fluctuations occur at the input stage of an SE resonant inverter, the resonant voltage applied to the IGBT can be directly affected, potentially exceeding the breakdown voltage of the IGBT, resulting in its failure. Consequently, the resonant voltage should be limited to below a safety threshold—hardware resonant voltage limiting methods are generally used to do so. This paper proposes a sensorless resonant voltage control method that limits the increase in the resonant voltage caused by overvoltage or supply voltage fluctuations. By calculating and predicting the resonance voltage through the analysis of the resonance circuit, the resonance voltage is controlled not to exceed the breakdown voltage of the IGBT. The experimental results of a 1.35 kW SE resonant inverter for a high-pressure induction heating rice cooker were used to verify the validity of the proposed sensorless resonant voltage limiting method.

Keywords: induction; heating; cooker; resonant inverters; sensorless control; resonant voltage control

Citation: Oh, Y.; Yeon, J.; Kang, J.; Galkin, I.; Oh, W.; Cho, K. Sensorless Control of Voltage Peaks in Class-E Single-Ended Resonant Inverter for Induction Heating Rice Cooker. *Energies* **2021**, *14*, 4545. https://doi.org/10.3390/en14154545

Academic Editor: Mario Marchesoni

Received: 24 June 2021
Accepted: 21 July 2021
Published: 28 July 2021

1. Introduction

Induction heating—that is, the conversion of electrical energy into thermal energy using electromagnetic induction generated in conductive materials in alternating magnetic fields—has been used in the melting and heat treatment of metals in industry for many years [1]. In particular, owing to the rapid progress of semiconductor devices and control systems in the 1980s, various high-frequency resonant inverter systems [2] have been developed as induction heating power sources. Their use has been increasing in industrial applications as well as in domestic cookers [3].

Inverters for domestic induction heating products, such as electric or induction rice cookers, usually have a capacity of 1–2 kW, using simple, low-cost, class-E single-ended (SE) resonant inverters [4]. Such inverters require a semiconductor switch with a high breakdown voltage—deemed to be necessary because a capacitor is connected in parallel with a working coil to obtain voltage resonance, which is applied to a switch in series with a DC link capacitor [5]. Consequently, an insulated-gate bipolar transistor (IGBT) with a high breakdown voltage of 1200 V or more is typically used as the switching element [6,7].

For the stable operation of a resonant inverter, it is necessary to stabilize the DC link voltage. Moreover, the power factor of the power input should be considered, making it

necessary to apply a DC/DC converter with a power factor correction function and a large capacitor in the DC link stage [8,9].

However, in the case of an SE resonant inverter, only a choke coil and a small capacitor to bypass a resonant current are applied to the bridge circuit DC stage—a method of using the high-input power factor characteristics of high-frequency switching on the inverter side [10,11], and the theoretical analysis of the equivalent circuit was presented [11,12]—simplifying the configuration circuit and reducing manufacturing costs. However, its small capacity makes it vulnerable to changes in the input voltage and distortion. Therefore, when the input power voltage fluctuates, the DC link voltage can be directly affected—that is, the resonant voltage and the voltage across the switching element may suddenly increase, destroying the switching element [13–15]. Consequently, for stable operation of an SE resonant inverter, it is necessary to control or limit the resonant voltage.

An active clamped class-E (ACCE) inverter that clamps the resonant voltage has been proposed as a solution. Although the output power of the ACCE inverter is lower than that of existing class-E inverters, it has the advantage of protecting the switching element by reducing the resonance voltage of the switch [16,17].

A hybrid scheme has been proposed to overcome the shortcomings of ACCE inverters with reduced output power [18], a method that has the advantage of increasing the output power by using two circuits—that is, a class-E and an ACCE inverter. However, these hybrid-ACCE inverters have the disadvantage of being more expensive than conventional class-E inverters because of the addition of auxiliary switches and clamping capacitors. To solve this problem, an improved hybrid-ACCE inverter control scheme using pulse frequency modulation and eliminating auxiliary frequency switches and clamping capacitors has been proposed [19]. Here, the switching frequency is adjusted based on the input reference voltage: the switching frequency of the class-E inverter is divided into constant frequency and variable frequency regions, the voltage stress of the switch being controlled by the variable frequency. However, this also requires more switches than the class-E inverter, increasing its price. Moreover, control is complex, raising the possibility of malfunctions. A prediction model of an induction heating inverter was made and the power was controlled, but the resonance voltage was not controlled [20].

In a steady-state, operation for induction heating is sufficient for use with SE inverters as well. However, when instantaneous fluctuations and disturbances occur in the field, the SE inverter is greatly affected compared to inverters of other topologies. The authors have also proposed a resonant voltage limitation method using hardware [21] comprising one current sensing resistor, one analog comparator, one set/reset (SR) latch, and one AND-gate. It is simple hardware but more complex to implement than software.

When an oversized load is operated in a grid, fluctuations and disturbances in the input voltage are inevitably accompanied. In this case, the SE inverter is frequently stopped because of the protective operation to prevent damage to the IGBT. Additionally, the heating time is increased. Therefore, the resonant voltage must be controlled in an abnormal state rather than in a steady state.

2. Methodology: Single-Ended (SE) Resonant Inverter for Induction Heating Rice Cooker

Figure 1 shows a circuit diagram of an SE resonant inverter used for induction heating. This inverter can significantly reduce switching losses through a zero-voltage switching operation, while the voltage across the IGBT, Q, is high owing to the voltage resonance. The input stage consists of a bridge diode for rectification, a choke coil, and a DC link capacitor, C_{dc}. An equivalent inductor, L_{eq}, and equivalent resistance, R_{eq}, for the working coil and cooking vessel are connected in series. A resonant capacitor, C_r, is connected in parallel with the working coil to form a resonant tank. In rice cookers, variations in the equivalent inductance and resistance are not significant as the rice cooking vessel is fixed within the cooker body with the working coil wound around it.

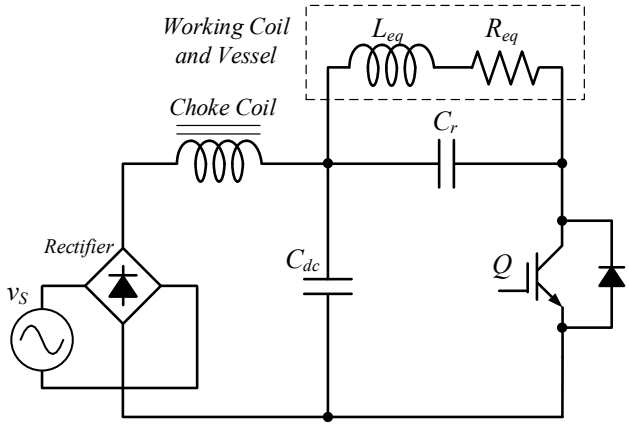

Figure 1. The circuit of a single-ended (SE) resonant inverter for induction heating.

2.1. Operation Mode of the Equivalent Resonant Circuit

The operation of the resonant inverter is shown in Figure 2. In mode I, the resonant current of the previous mode flows through the anti-parallel diode of the switching element Q. Consequently, the voltage across the switching element, Q, is zero. The switching device is turned on during this period, and zero-voltage switching is performed. Mode II is an operational mode in which the switching element, Q, is turned on to receive power from the input while the current flows through the equivalent inductor, L_{eq}, and equivalent resistor, R_{eq}. In Mode III, the switching element, Q, is turned off, and resonance starts between the equivalent inductor L_{eq} and resonant capacitor C_r. In this case, neglecting the tail current of the IGBT used as a switching element can be considered to be zero-voltage turn-off switching. Mode IV is an operational mode in which the energy of the equivalent inductor, L_{eq}, is accumulated in the resonant capacitor C_r and then transferred to the equivalent inductor L_{eq} [22].

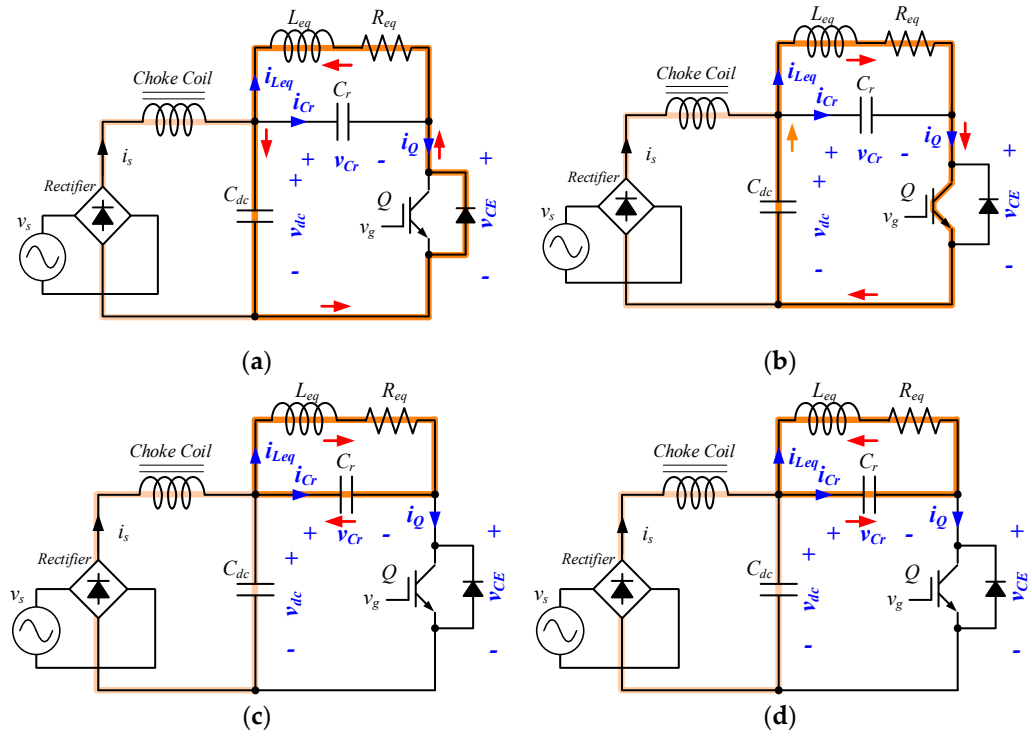

Figure 2. Operation modes of the single-ended (SE) resonant inverter: (**a**) mode I (t_0~t_1); (**b**) mode II (t_1~t_2); (**c**) mode III (t_2~t_3); (**d**) mode IV (t_3~t_0).

Figure 3 shows the theoretical voltage and current waveforms of each part of the circuit during operation.

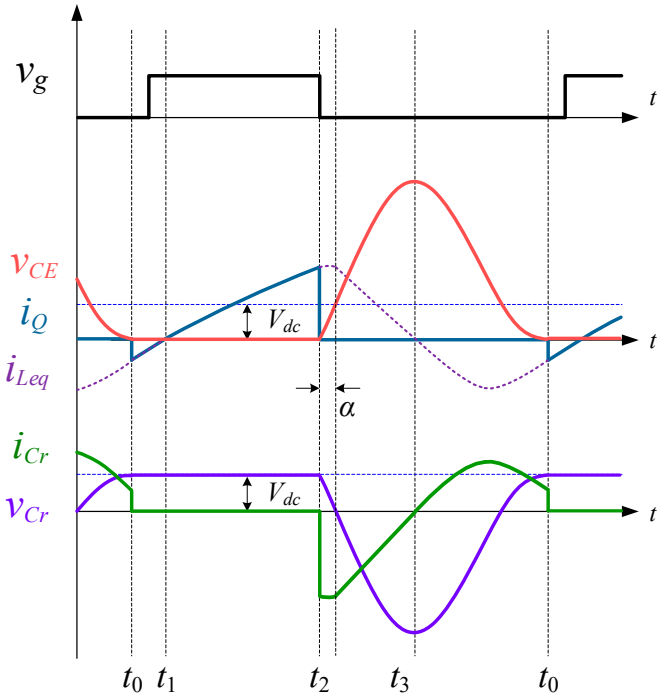

Figure 3. Theoretical waveforms of the single-ended (SE) resonant inverter.

2.2. Anlalysis of the Equivalent Resonant Circuit

Two equivalent circuits of the inverter exist, as shown in Figure 4: one for the on-state of the IGBT and another for the off-state [22].

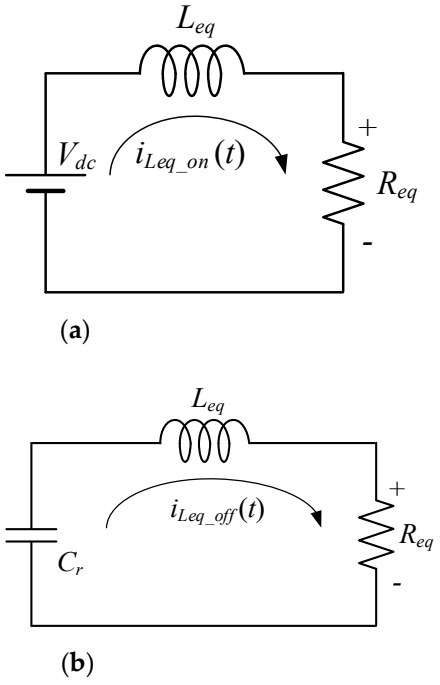

Figure 4. Equivalent circuits of switching device Q status of the SE resonant inverter: (**a**) equivalent circuit for the switching device, Q, in turned-on status; (**b**) equivalent circuit for the switching device, Q, in turned-off status.

When the IGBT, Q, is turned on, the current flows through the equivalent inductor L_{eq} and equivalent resistance R_{eq}, as shown in Figure 4a. When the IGBT, Q, is turned off, the inductor energy is transferred to the capacitor by resonance, as shown in Figure 4b.

First, assuming that the DC link voltage, V_{dc}, is constant while the switching element, Q, is turned on, it is possible to compose the voltage equation of the equivalent circuit, as follows:

$$V_{dc} = L_{eq}\frac{d\, i_{Leq\_on}(t)}{dt} + R_{eq}\, i_{Leq\_on}(t) \tag{1}$$

The inductor current, i_{Leq_on}, can be derived from (1), which in the case of the on-state, can be represented as:

$$i_{Leq\_on}(t) = \frac{V_{dc}}{R_{eq}}\left(1 - e^{-\frac{R_{eq}}{L_{eq}}t}\right) \tag{2}$$

When the IGBT, Q, is off, the current of equivalent inductor L_{eq} continues flows as shown in Figure 4b. The voltage equation of the equivalent circuit can be expressed as:

$$\frac{1}{C_r}\int i_{Leq\_off}\, dt + L_{eq}\frac{d}{dt}i_{Leq\_off} + R_{eq}\, i_{Leq\_off} = 0 \tag{3}$$

When the IGBT, Q, is turned on, the inductor current, i_{Leq_off}, can be represented as:

$$i_{Leq\_off}(t) = Ae^{-\alpha t}\cos(\omega t + \theta) \tag{4}$$

where:

$$A = \sqrt{\left(\frac{V_{dc}}{\omega L_{eq}} - \frac{\alpha I_{LeqP}}{\omega}\right)^2 + {I_{LeqP}}^2} \tag{5}$$

$$\alpha = \frac{R_{eq}}{2L_{eq}} \tag{6}$$

$$\omega = \sqrt{\frac{1}{L_{eq}C_r} - \left(\frac{R_{eq}}{2L_{eq}}\right)^2} \tag{7}$$

and

$$\theta = \tan^{-1}\left(\frac{\alpha L_{eq} I_{LeqP} - V_{dc}}{\omega L_{eq} I_{LeqP}}\right) \tag{8}$$

Conversely, when the switching element, Q, is turned off, the resonance of the equivalent inductor, L_{eq}, and resonant capacitor, C_r, starts; therefore, the resonant capacitor current i_{Cr} can be expressed as follows:

$$i_{Cr\_off}(t) = -i_{Leq\_off}(t) \tag{9}$$

$$= -Ae^{-\alpha t}\cos(\omega t + \theta) \tag{10}$$

Accordingly, the resonant capacitor voltage, v_{Cr}, can be represented as follows:

$$v_{Cr}(t) = \frac{1}{C_r}\int i_{Cr}(t)dt \tag{11}$$

$$= -\frac{A}{C_r}\int e^{-\alpha t}\cos(\omega t + \theta)dt \tag{12}$$

As the maximum instant of the resonance voltage is a quarter of the resonance period, T, the value of the peak resonance voltage, V_{CrP}, can be derived as follows:

$$V_{CrP} = \frac{1}{C_r}\int_0^{\frac{T}{4}} i_{Cr}(t)dt \tag{13}$$

$$= -\frac{A}{C_r}\int_0^{\frac{T}{4}} e^{-\alpha t}\cos(\omega t+\theta)dt \tag{14}$$

$$= -\frac{A}{C_r}\frac{1}{(\alpha+\omega)^2}\left(\alpha+\omega e^{-\frac{\alpha\pi}{2\omega}}\right) \tag{15}$$

The voltage across the switching element v_{CE} is the sum of the DC link voltage and resonant capacitor voltage. Thus, v_{CE} can be given by:

$$v_{CE}(t) = V_{dc} - v_{Cr}(t) \tag{16}$$

Consequently, the maximum value, V_{CEM}, that appears across the IGBT over the entire period of the source voltage, v_S, can be given by:

$$V_{CEM} = V_{SP} - V_{CrP} \tag{17}$$

where V_{SP} is the maximum value of the source voltage, v_S.

As shown in (15), the maximum voltage, V_{CEM}, is usually 1000 V or more because V_{CrP} is negative, making it necessary to control the magnitude of the resonance voltage to prevent breakage of the IGBT.

2.3. Sensorless Control of Voltage Peaks by Resonant Voltage Estimation Using the Turn-On Duration of the IGBT

We can calculate the resonant peak voltage, V_{CrP}, using (15). However, it is complex, and calculations using (15) can be a burden on the MCU.

As ω >> α, A and V_{CrP} in (5) and (15) can be represented, respectively, as:

$$A \approx I_{LeqP} \tag{18}$$

$$V_{CrP} \approx -\frac{A}{C_r}\frac{1}{(\alpha+\omega)} \tag{19}$$

Meanwhile, the peak current of the working coil is equal to the current at the turn-off instant of the IGBT. As the conduction period of the anti-parallel diode before the IGBT turns on is relatively short, it can be ignored. Consequently, the peak current of the working coil, I_{LeqP}, can be obtained from the DC link voltage, V_{dc}, the equivalent inductance, L_{eq}, and the turn-on duration of the switching element, t_{on}, as follows:

$$I_{LeqP} = \frac{V_{dc}\times t_{on}}{L_{eq}} \tag{20}$$

The peak resonant voltage can be given by:

$$V_{CrP} \approx -\frac{V_{dc}\times t_{on}}{L_{eq}C_r(\alpha+\omega)} \tag{21}$$

It can be seen that (21) is simpler to calculate than (15). Substituting (21) into (17) yields:

$$V_{CEM} \approx V_{SP} + \frac{V_{SP}\times t_{on}}{L_{eq}C_r(\alpha+\omega)} \tag{22}$$

The turn on time can be given by:

$$t_{on} = \frac{(V_{CEM}-V_{SP})L_{eq}C_r(\alpha+\omega)}{V_{SP}} \tag{23}$$

Typically, the SE converter controls the input power by measuring the input voltage and current, as it is easier to measure the low-frequency than the high-frequency AC of the output. With the input voltage and turn-on time, the resonant voltage can be controlled

using (21) without any additional circuits, including a voltage sensor for the high-frequency resonant voltage. Consequently, the maximum voltage across the IGBT can be limited using (22).

The constants of the equivalent variables and switching frequency change slightly during operation, making it difficult to calculate the resonant peak voltage, V_{CrP}, using (15). Consequently, we propose a simple estimation method to control the resonant voltage for the protection of the switching element from overvoltage damage.

Figure 5 shows the sequence for power control and resonance voltage control. MCU performs AD conversion at 100 us interrupt, which is the control cycle.

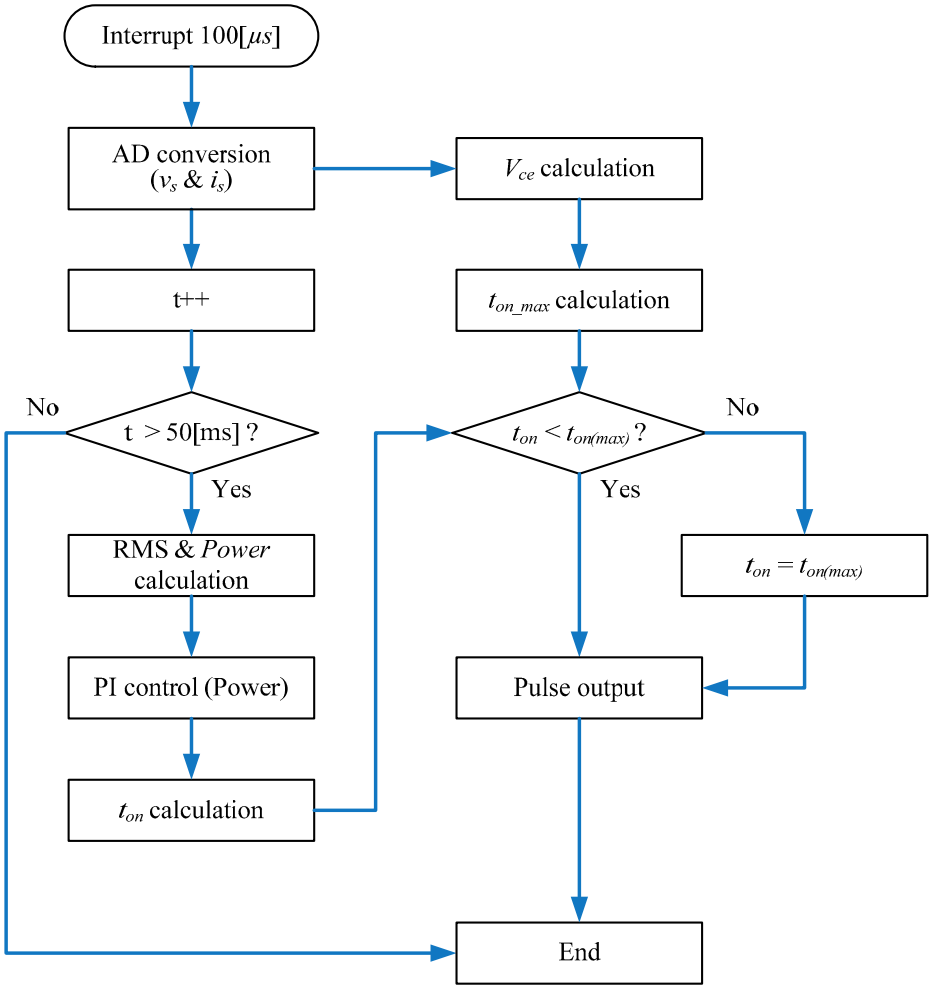

Figure 5. Sequence flowchart for resonant voltage control.

The ton is calculated every 50 ms by executing the PI controller. The t_{off} is determined according to the working coil and vessel and is a fixed value. Therefore, the period of PWM becomes t_{on} + t_{off}, so the switching frequency slightly varies according to the amount of power. The maximum value of ton, $t_{on(max)}$, is calculated by Equation (23). V_{CEM} is determined in consideration of the breakdown voltage of the IGBT. If the PWM ton is greater than a $t_{on(max)}$, the t_{on} is limited to $t_{on(max)}$.

3. Results: Experimental Setup and Evaluation

Figure 6 shows the configuration of the SE resonant inverter of the 1.35 kW household induction rice cooker used in the experiment, an MC56F8002 being used as a controller in the experimental setup. Table 1 and Figure 7 show the parameters of the experimental setup and an image of the main printed circuit board (PCB), respectively.

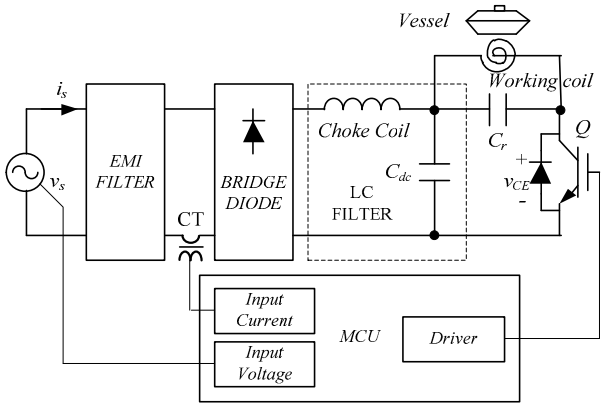

Figure 6. Configuration of the single-ended (SE) resonant inverter for the 1.35 kW domestic induction rice cooker used in the experiment.

Table 1. Parameters of the experimental setup.

Parameter	Value
Rated source voltage	220 [V]
Rated source current	6.14 [A]
Rated input power	1350 [W]
Ratings of bridge diode	600 [V]/15 [A]
Inductance of chock coil	660 [μH]
Capacitance of C_r	0.22 [μF]
Inductance of L_{eq}	90 [μH]
Resistance of R_{eq}	4 [Ω]
Frequency of f_s	24–50 [kHz]
Ratings of switching IGBT	1350 [V]/30 [A]

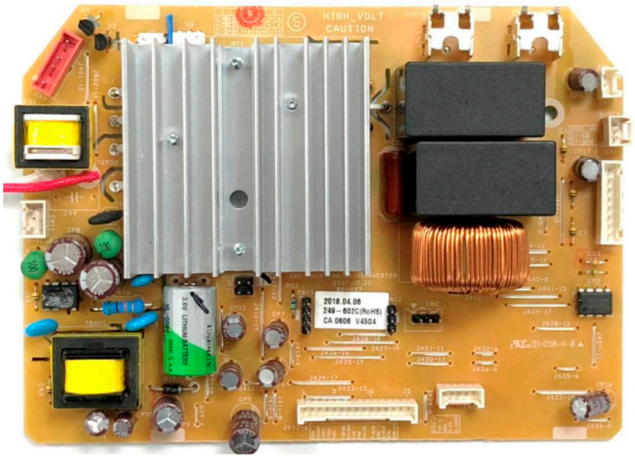

Figure 7. Image of the main printed circuit board (PCB).

First, waveforms of the voltage across the switching element, v_{CE}, and the resonant current, i_{Leq}, with a source voltage of 220 V, are shown in Figure 8. The maximum voltage across the switching element was measured to be 1016 V, approximately 75% of the IGBT ratings used in the experiment.

The experiment was conducted under fluctuations of the source voltage to verify the usefulness of the proposed resonant voltage estimation method, the source voltage fluctuations being induced by increasing it from 220 V to 260 V for 1 ms (using the 80° voltage phase).

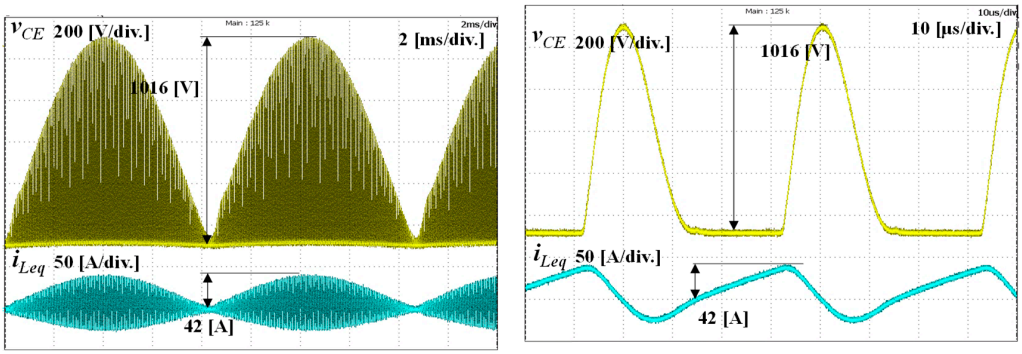

(**a**) (**b**)

Figure 8. Experimental waveforms under a normal source voltage (220 V): (**a**) waveforms of v_{CE} and i_{Leq}; (**b**) enlarged waveforms at peak positions.

The experimental results—using the single-ended (SE) resonant inverter shown in Figures 5 and 6—under source voltage fluctuations, are shown in Figure 9. In these experiments, the source voltage was increased at the disturbance point, the reaction of the inverter being recorded.

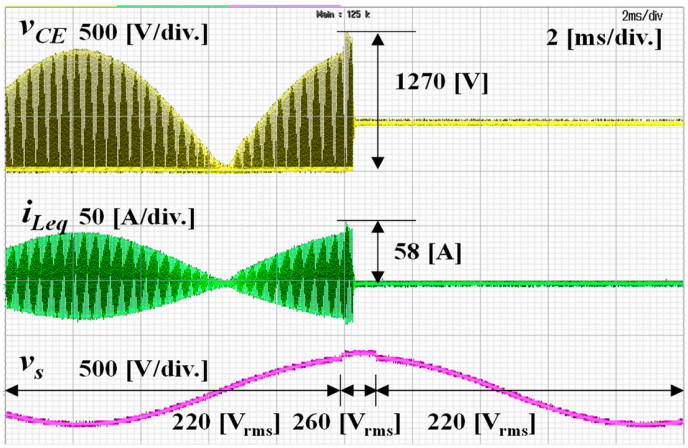

(**a**)

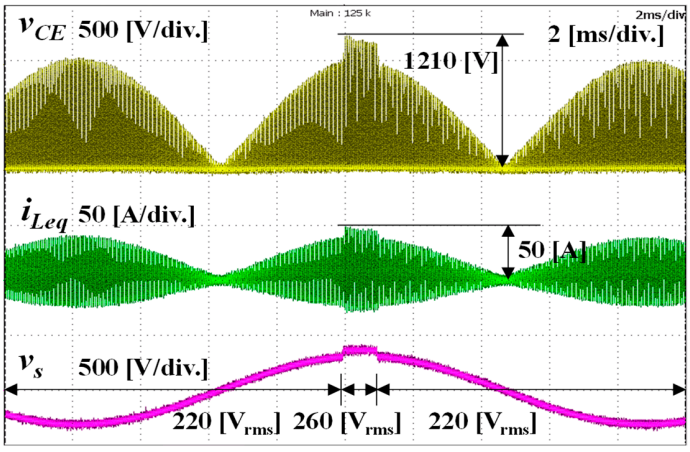

(**b**)

Figure 9. Experimental waveforms under source voltage fluctuations: (**a**) a conventional system; (**b**) the proposed system.

The results of the conventional system without resonant-voltage limit-control under source voltage disturbance are shown in Figure 9a. These show that the inverter tripped owing to the IGBT overvoltage protection at the voltage disturbance point. In this case, the overvoltage level was 1270 V, the voltage safety margin being just 80 V for the 1350 V-rated IGBT.

Figure 9b shows the experimental results of the proposed sensorless method, the voltage across the IGBT being limited to a specific level. As a result, the inverter operated continuously without tripping. In this case, the control level of the resonant peak voltage was set to 900 V, the peak voltage across the IGBT being limited to 1210 V. Here, the voltage margin was 140 V, the peak voltage across the IGBT level being 90% of the IGBT rating. Consequently, it was confirmed that the proposed system could be operated stably and continuously without tripping under voltage disturbances.

Figure 10 shows the experimental results of a resonant voltage limitation method using the hardware proposed in [19]. The performance of the proposed sensorless method and that of the hardware method are the same as those shown in Figures 9 and 10. The hardware comprises one current sensing resistor, one analog comparator, one SR latch, and one AND-gate, as shown in Figure 10b. It is simple, but more expensive, hardware. As most home appliances today use an MCU as a controller, it is desirable to have as few components as possible.

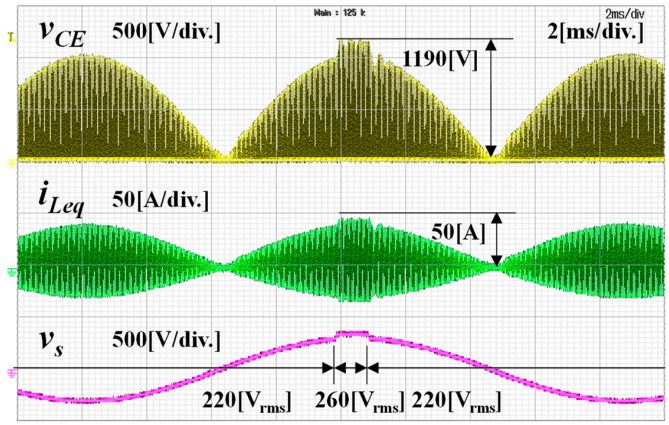

(**a**)

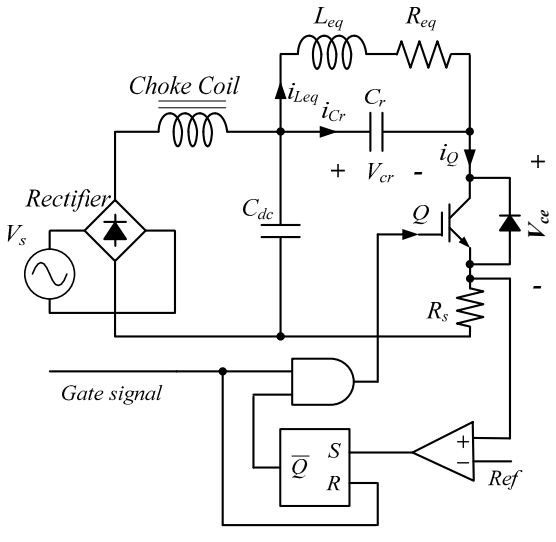

(**b**)

Figure 10. Experimental result using hardware limitation: (**a**) experimental waveforms; (**b**) circuit diagram.

4. Discussion

The given results showed that the voltage across the switching element of the SE resonant inverter could be limited to a certain level or less using the proposed sensorless resonant voltage peak control. As a result, the inverter could be operated continuously without tripping. When the control level of the resonant peak voltage was set to 890 V, the peak voltage across the switching element was limited to 1200 V. This result indicates that the proposed method could provide stable control even under input voltage fluctuations and disturbances by limiting the high-voltage stress across the switching element. The system efficiency was 96.55% at full load and 88.13% at 40% load. While the input voltage is rising, it operates as hard switching, not ZVS. However, since the resonance voltage peak control is operated under abnormal, the efficiency is not affected.

5. Conclusions

In this paper, a sensorless resonance voltage estimation method is proposed to prevent the breakdown of IGBT in case of instantaneous fluctuation of input voltage and to enable continuous operation without protection operation. The validity of the proposed method was verified experimentally using an SE resonant inverter for a 1.35 kW induction heating household rice cooker.

The proposed method has the advantage to implement without additional hardware or high-frequency side voltage sensors in an SE inverter. Since resonant voltage estimation requires input voltage and turn-on time, it can be easily calculated even with a low-cost MCU. However, it is necessary to consider the change in circuit constant in actual application due to temperature rise.

Author Contributions: Conceptualization, Y.O. and J.Y.; methodology, Y.O. and J.Y.; software, J.K.; validation, W.O., I.G., and K.C. writing—original draft preparation, W.O. and K.C.; writing—review and editing, I.G., W.O., and K.C. All authors have read and agreed to the published version of the manuscript.

Funding: This research received no external funding.

Conflicts of Interest: The authors declare no conflict of interest.

References

1. Dawson, F.; Jain, P. A comparison of load commutated inverter systems for induction heating and melting applications. *IEEE Trans. Power Electron.* **1991**, *6*, 430–441. [CrossRef]
2. Bi, C.; Lu, H.; Jia, K.; Hu, J.; Li, H. A Novel Multiple-Frequency Resonant Inverter for Induction Heating Applications. *IEEE Trans. Power Electron.* **2016**, *31*, 8162–8171. [CrossRef]
3. Kim, D.; So, J.; Kim, D. Study on Heating Performance Improvement of Practical Induction Heating Rice Cooker with Magnetic Flux Concentrator. *IEEE Trans. Appl. Supercond.* **2016**, *26*, 1–4. [CrossRef]
4. Bhasme, N.R.; Mandval, B. Topologies of Voltage Source Inverter for Domestic Induction Heating. *J. Sci. Eng. Res.* **2015**, *6*, 121–126.
5. Yeon, J.; Park, M.; Cho, K.; Kim, H. Field stop shorted anode trench IGBT for induction heating appliances. In Proceedings of the 38th Annual Conference on IEEE Industrial Electronics Society (IECON 2012), Montreal, QC, Canada, 25–28 October 2012; pp. 422–426. [CrossRef]
6. Yeon, J.; Park, M.; Cho, K.; Kim, H. A new high voltage shorted-anode IGBT with intrinsic body diode improves performance of single-ended induction cooker. In Proceedings of the 15th European Conference on Power Electronics and Applications (EPE 2013), Lille, France, 2–6 September 2013; pp. 1–9. [CrossRef]
7. Crisafulli, V. New IHR Field Stop II IGBT technology, the best efficiency for high frequency Induction Cooking Applications. In Proceedings of the International Exhibition and Conference for Power Electronics, Intelligent Motion, Renewable Energy and Energy Management (PCIM Europe 2014), Nuremberg, Germany, 20–22 May 2014; pp. 873–880.
8. Tanimatsd, H.; Ahmed, T.; Hirota, I.; Yasui, K.; Iwai, T.; Omori, H.; Ahmed, N.; Lee, H.; Nakaoka, M. Two-switch boost-half bridge and boost active clamped ZVS-PWM AC-AC converters for consumer high frequency induction heater. In Proceedings of the Twentieth Annual IEEE Applied Power Electronics Conference and Exposition (APEC 2005), Austin, TX, USA, 6–10 March 2005; Volume 2, pp. 1124–1130. [CrossRef]
9. Pérez-Tarragona, M.; Sarnago, H.; Lucía, Ó.; Burdío, J. Design and Experimental Analysis of PFC Rectifiers for Domestic Induction Heating Applications. *IEEE Trans. Power Electron.* **2018**, *33*, 6582–6594. [CrossRef]

10. Fairchild Semiconductor. *Induction Heating System Topology Review, AN-9012, Rev 1.0.4 12/18/13*; Fairchild Semiconductor: Sunnyvale, CA, USA, 2000.
11. Yeon, J.; Cho, K.; Kim, H. A 3.6 kW Single-ended Resonant Inverter for Induction Heating Applications. In Proceedings of the 17th European Conference on Power Electronics and Applications (EPE'15 ECCE-Europe), Geneva, Switzerland, 8–10 September 2015; pp. 1–7. [CrossRef]
12. Sarnago, H.; Lucía, O.; Mediano, A.; Burdío, J.M. A Class-E Direct AC–AC Converter With Multicycle Modulation for Induction Heating Systems. *IEEE Trans. Ind. Electron.* **2014**, *61*, 2521–2530. [CrossRef]
13. Lucia, O.; Burdio, J.; Millan, I.; Acero, J.; Puyal, D. Load-Adaptive Control Algorithm of Half-Bridge Series Resonant Inverter for Domestic Induction Heating. *IEEE Trans. Ind. Electron.* **2009**, *56*, 3106–3116. [CrossRef]
14. Kim, C. Minimization of Abnormal Output Voltage Rising for LLC Resonant Converter at Very Light Load. *IEEE Trans. Ind. Electron.* **2019**, *67*, 1–9. [CrossRef]
15. Cai, M.; Wasynczuk, O.; Saeedifard, M. A Voltage- Edge-Rate-Limiting Soft-Switching Inverter Based on Auxiliary Resonant Pole. *IEEE J. Emerg. Sel. Top. Power Electron.* **2019**, *7*, 736–744. [CrossRef]
16. Divan, D.; Skibinski, G. Zero-Switching-Loss Inverters for High-Power Applications. *IEEE Trans. Ind. Appl.* **1989**, *25*, 634–643. [CrossRef]
17. Kim, H.; Leu, C.; Farrington, R.; Lee, F. Clamp Mode Zero-Voltage-Switched Multi-Resonant Converters. In Proceedings of the 23rd Annual IEEE Power Electronics Specialists Conference (PESC 1992), Toledo, Spain, 29 June–3 July 1992; pp. 18–24. [CrossRef]
18. Lee, D.; Hyun, D. A new hybrid Control Scheme Using Active-Clamped Class-E Inverter with Induction Heating Jar for High Power Application. In Proceedings of the 17th Annual IEEE Applied Power Electronics Conference and Exposition (APEC 2002), Dallas, TX, USA, 10–14 March 2002; Volume 2, pp. 1148–1153. [CrossRef]
19. Park, N.; Lee, D.; Hyun, D. A Study on the New Control Scheme of Class-E Inverter for IH-Jar Application with Clamped Voltage Characteristics Using Pulse Frequency Modulation. *IET Electr. Power Appl.* **2007**, *1*, 433–438. [CrossRef]
20. Kranprakon, P.; Sangswang, A.; Naetiladdanon, S. Model predictive control of LLC resonant inverter for induction furnace. In Proceedings of the 2017 International Electrical Engineering Congress (IEECON), Pattaya, Thailand, 8–10 March 2017; pp. 1–4. [CrossRef]
21. Oh, Y.; Yeon, J.; Cho, K.; Kim, H. Resonant voltage limiting technique of single-ended resonant inverter for induction heating. *Electron. Lett.* **2017**, *53*, 804–806. [CrossRef]
22. Oh, Y.; Cho, K. Load State Detection Method of the Single-Ended Resonant Inverter for the Induction Heating Rice Cooker. *J. Korean Inst. Inf. Technol.* **2020**, *18*, 43–54. [CrossRef]